Comparing the Diagnostic Potential of ^{68}Ga-Alfatide II and ^{18}F-FDG in Differentiating Between Non–Small Cell Lung Cancer and Tuberculosis

Fei Kang*[1], Shengjun Wang*[1], Feng Tian*[2], Mingxuan Zhao[1], Mingru Zhang[1], Zhe Wang[1], Guoquan Li[1], Changli Liu[3], Weidong Yang[1], Xiaofei Li†[2], and Jing Wang†[1]

[1]Department of Nuclear Medicine, Xijing Hospital, Fourth Military Medical University, Xi'an, China; [2]Department of Thoracic Surgery, Tangdu Hospital, Fourth Military Medical University, Xi'an, China; and [3]Tuberculosis Hospital of Shaanxi Province, Xi'an, China

The objectives of this study were to compare the diagnostic potential of ^{68}Ga-Alfatide II with ^{18}F-FDG in differentiating between non–small cell lung cancer patients (NSCLC) and lung tuberculosis (TB) patients. **Methods:** Twenty-one NSCLC patients and 13 TB patients were recruited. PET/CT images using either ^{68}Ga-Alfatide II or ^{18}F-FDG were acquired in 2 consecutive days. SUV quantitative comparison, receiver-operating curve analysis, and comprehensive visual analysis were performed. The expression of the angiogenesis marker $\alpha_v\beta_3$ in NSCLC and TB primary lesions was analyzed by immunohistochemistry. **Results:** The ^{68}Ga-Alfatide II SUV_{max} and SUV_{mean} were significantly different in NSCLC and TB ($P = 0.0001$ and 0.0007, respectively). The area under the receiver-operating curve value of ^{68}Ga-Alfatide II SUV_{max} was significantly higher than that of ^{18}F-FDG ($P = 0.038$). The visual differentiation diagnostic specificity of ^{68}Ga-Alfatide II was 1.57-fold (84.62% vs. 53.85%) higher than that of ^{18}F-FDG. In the detection of NSCLC lymph nodes, ^{68}Ga-Alfatide II was superior in specificity (100% vs. 66.7%), whereas the sensitivity was greater with ^{18}F-FDG (87.5% vs. 75%). In TB lymph node detection, the false-positive rate of ^{68}Ga-Alfatide II was one-third (15.4%/46.2%) the value of ^{18}F-FDG. Additionally, ^{68}Ga-Alfatide II detected more metastases in the brain but less in the liver and the bone. The $\alpha_v\beta_3$ biomarker was specifically expressed in the cells and the neovasculature of NSCLC lesions. **Conclusion:** ^{68}Ga-Alfatide II is qualified for detecting NSCLC primary lesions and is superior to ^{18}F-FDG in distinguishing NSCLC from TB in primary lesions and suggestive lymph nodes. ^{68}Ga-Alfatide II is more likely to be capable of detecting brain metastasis, and ^{18}F-FDG is more likely to be capable of detecting liver and early-stage bone metastases.

Key Words: ^{68}Ga-Alfatide II; ^{18}F-FDG; non-small cell lung cancer; tuberculosis

J Nucl Med 2016; 57:672–677
DOI: 10.2967/jnumed.115.167924

Lung cancer is a leading cause of death by malignancy because of its high morbidity and mortality (*1*). Non–small cell lung cancer (NSCLC) accounts for more than 85% of all lung cancer cases (*2*). ^{18}F-FDG PET/CT has been well established as a crucial tool for detecting, identifying, and staging NSCLC, with obvious superiority compared with traditional anatomy imaging modalities (*2*). An SUV greater than 2.5 has been widely accepted as a cutoff value for differentiating lung malignancies from benign cases with ^{18}F-FDG (*3,4*). However, the specificity of ^{18}F-FDG PET/CT has been vigorously challenged. In clinical practice, it is not rare for benign lesions to represent an SUV higher than 2.5 and result in false-positive diagnoses (*5*).

Tuberculosis (TB), caused by *Mycobacteria*, infects one third of the world's population and often radiologically manifests like lung cancer (*5–7*). Such epidemic situations and radiographic features have made TB the unshakable leading cause of false-positive PET/CT lung cancer diagnoses in high-prevalence areas. In TB-epidemic regions, it was observed that TB resulted in 57.1%–92% of false-positive diagnoses of primary lung cancer and was also listed as one of the major false-positive causes of malignant lymph nodes (LNs) (*8–11*). The reason for this deficiency is mainly attributed to the ^{18}F-FDG tracer. Because of activated immune cells, the TB site also presents an elevated level of glucose consumption (*12*). Although efforts have been made, such as delayed image acquisition (*9,13*), this inherent shortcoming of ^{18}F-FDG has not been perfectly solved (*10*). New tracers targeting other distinct pathologic characteristics of NSCLC and TB will be an aid to noninvasively differentiate these 2 diseases and thus enhance the clinical accuracy of PET/CT.

Angiogenesis has immense potential as a differentiation target. In tumor lesions, induced by the strong demand of cancer cells and the abnormal microenvironment, neovasculature is abundant (*14,15*). In TB lesions, however, a recent morphologic study demonstrated a sharp decrease in microvessel density from the granuloma edge to the avascular central region (*16*). The thin-rim enhancement pattern of TB lesions in enhanced CT images also confirms the low-angiogenesis feature that is different from NSCLC (*7*).

Alfatide II [NOTA-E[PEG_4-c(RGDfk)]$_2$, an upgraded version of dimer RGD (Arg-Gly-Asp)-based tracer targeting the neovascular marker integrin $\alpha_v\beta_3$, has been proven to be of lower liver uptake and higher tumor accumulation in mice (*17*). Clinical data are required to understand whether this new RGD-based angiogenesis

Received Oct. 15, 2015; revision accepted Dec. 4, 2015.
For correspondence or reprints contact either of the following:
Jing Wang, Department of Nuclear Medicine, Xijing Hospital, Fourth Military Medical University, No.127 West Changle Road, Xi'an, P.R. China 710032.
E-mail: wangjing@fmmu.edu.cn
Xiaofei Li, Department of Thoracic Surgery, Tangdu Hospital, Fourth Military Medical University, 569 Xinsi Rd., Xi'an, P.R. China 710038.
E-mail: lxfchest@fmmu.edu.cn
*Contributed equally to this work.
†Contributed equally to this work.
Published online Dec. 30, 2015.

tracer can highlight NSCLC lesions as well as differentiate lung TB from NSCLC.

Herein, the diagnostic potential of ^{68}Ga-Alfatide II to identify NSCLC and TB patients was, to our knowledge, investigated for the first time and compared with the performance of ^{18}F-FDG by auto-control observation.

MATERIALS AND METHODS

Patients

This study was approved by the Ethics Committee of Xijing Hospital (approval no. 20131218-6) and conducted from September 2014 to January 2015. Written informed consent was obtained from each participating patient. This study was registered in the Chinese Clinical Trial Register (ChiCTR-DDT-14005083).

Twenty-one patients with NSCLC (7 women and 14 men) and 13 patients with lung TB (7 women and 6 men) were recruited. All patients exhibited a suggestive single lung mass lesion on their previous CT scan. The definite diagnosis of NSCLC was established by preoperational bronchoscopicor puncture biopsy in all the 21 enrolled patients and was finally confirmed by postoperational histopathology in 17 patients who received resection operations. According to the *Treatment Guidelines of Tuberculosis* compiled by World Health Organization (http://www.who.int/tb/publications/2010/9789241547833/en/), the definite diagnosis of TB was established by positive sputum culture in all the 13 enrolled patients and additionally by bronchoscopic biopsy in 4 of them. The response to antitubercular therapy on the follow-up CT scans, for at least 6 mo, was considered as collateral evidence for establishing the TB diagnosis and ruling out the comorbidity of NSCLC in TB patients.

No treatment or surgery was performed on any patients before they underwent PET/CT scans. All the biopsies were done at least 10 d before PET/CT scans to avoid the influence of puncture injury. The patients' information is summarized in Table 1.

^{68}Ga-Alfatide II and ^{18}F-FDG Preparation

The Alfatide II kit was produced in the National Institutes of Health based on a previously described protocol (*18*). ^{68}Ga was produced by a ^{68}Ge-^{68}Ga generator (ITG). The synthesis protocol of ^{68}Ga-Alfatide II is described in the supplemental materials (available at http://jnm.snmjournals.org). ^{18}F-FDG was produced by cyclotron using FDG reagent kits (ABX).

PET/CT Imaging

PET/CT imaging was performed on a Biograph 64 PET/CT scanner (Siemens). All the patients received ^{68}Ga-Alfatide II and ^{18}F-FDG PET/CT scans on 2 consecutive days. ^{68}Ga-Alfatide II and ^{18}F-FDG were injected intravenously with a dosage of 1.85 MBq/kg (0.05 mCi/kg) and 5.55 MBq/kg (0.15 mCi/kg), respectively. The dosage was determined on the basis of previous clinical trials (*19,20*). Whole-body PET imaging was acquired 60 min after the injection of tracers.

TABLE 1
Basic Information of Patients

Grouping	Number	Male	Female	Mean age ± SD (y)
NSCLC group	21	14	7	52.0 ± 10.1
Adenocarcinoma	15	8	7	52.6 ± 10.9
Squamous carcinoma	6	6	0	53.8 ± 9.3
TB group	13	6	7	36.5 ± 15.1
Total	34	20	14	42.4 ± 15.6

Image Analysis

The image analysis and comparison method was partly based on the methods of previous reports (*21,22*). Three-dimensional regions of interest were drawn over the lung lesions and any abnormal LNs or metastatic lesions. The tracer uptake level was expressed in SUV.

For the quantitative comparison of the 2 tracers, the SUV_{max} and SUV_{mean} of the lung lesions were recorded, and Mann–Whitney nonparametric tests were used to compare the SUV data from the 2 groups of patients.

Receiver-operating-characteristic (ROC) curve analysis was performed to further assess the performance of the 2 tracers in differentiating TB from NSCLC. The area under the ROC curve (AUC) was calculated to evaluate the discriminant function of each tracer, and a cutoff value was, respectively, determined in the point of the highest Youden index (sensitivity + specificity − 1).

Furthermore, PET/CT diagnosis not only depends on SUV, but also is a comprehensive task performed by physicians who assess PET and CT signs and parameters together. For a comprehensive visual comparison, PET/CT images were viewed by 3 experienced nuclear medicine physicians through consensus reading and blinded to the history and pathologic diagnosis. The image quality, number of lesions, and diagnoses (malignant or TB) were recorded. The sensitivity, specificity, positive predictive value, and negative predictive value were used to compare the difference in efficacy of the 2 tracers.

Immunohistochemistry

The immunohistochemistry procedure is described in the supplemental materials.

Statistical Analysis

All data were analyzed by GraphPad Prism 5.0 (GraphPad Software) and presented as mean ± SD. Differences between the 2 groups were determined by Mann–Whitney nonparametric tests. Differences between the 2 AUC values in ROC analysis were determined by Z tests, as reported by Hanley and McNeil (*23*). A P value of less than 0.05 was considered statistically significant.

RESULTS

^{68}Ga-Alfatide II Preparation

The structure of Alfatide II is shown in Supplemental Figure 1. The ^{68}Ga labeling of Alfatide II was completed within 10 min, with a radiochemical purity of more than 95% (Supplemental Fig. 2). The administered mass of ^{68}Ga-Alfatide II was 8.2 ± 1.2 μg (range, 6.2–10.7 μg). The mean administered activity was 118.4 ± 29.6 MBq (3.2 ± 0.8 mCi). There were no adverse or clinically detectable pharmacologic effects in any of the 34 patients.

Distribution of ^{68}Ga-Alfatide II in Lung Cancer Patients

The imaging quality of ^{68}Ga-Alfatide II was good in all the patients. The distribution overviews of ^{68}Ga-Alfatide II and ^{18}F-FDG are demonstrated through coronal PET projections of a representative lung cancer patient in Figure 1. Except for the intense uptake in the kidneys and bladder for its urine excretion pathway, ^{68}Ga-Alfatide II mainly accumulated in NSCLC lesions. The background of the normal lung, heart, and mediastinum was quite low, allowing for clear observation of the abnormal hotspots in the lung. Nonspecific uptake could be observed in the liver, spleen, intestines, and the nasopharyngeal region. Compared with ^{18}F-FDG, ^{68}Ga-Alfatide II featured in the clear background of the brain and mediastinum, which may highlight the lesions or metastases in these regions in a better way. The nonspecific uptake of ^{68}Ga-Alfatide II of increased intensity in the abdomen indicated its relative disadvantage in abdominal lesions.

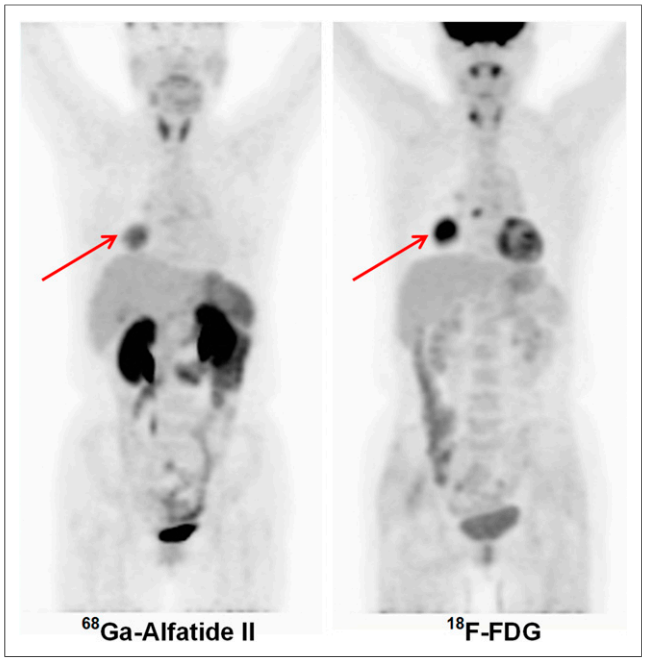

FIGURE 1. Distribution overview of ^{68}Ga-Alfatide II and ^{18}F-FDG in representative squamous carcinoma patient. Tumors are indicated by red arrows.

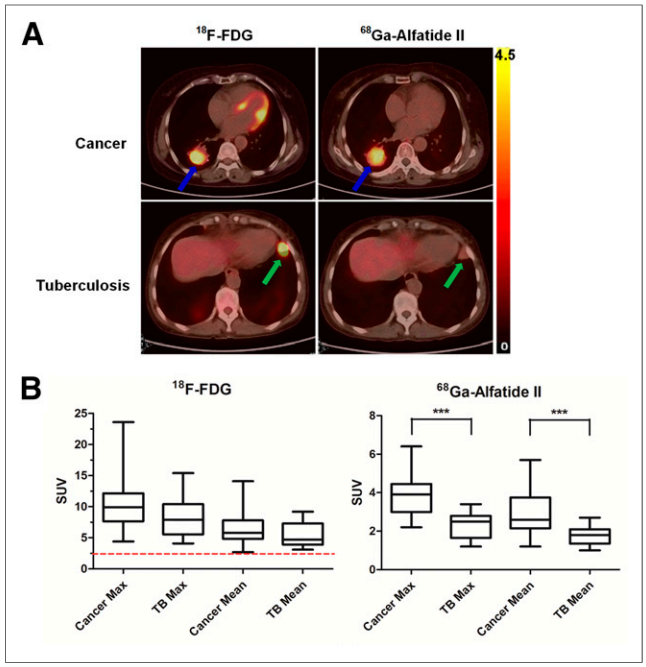

FIGURE 2. (A) Representative transaxial ^{18}F-FDG and ^{68}Ga-Alfatide II PET/CT images in same NSCLC or TB patient. Cancer is indicated by blue arrows. TB lesion is indicated by green arrows. (B) Quantitation of SUV_{max} and SUV_{mean} of cancer and TB primary lesions that were imaged by ^{18}F-FDG and ^{68}Ga-Alfatide II. Red dotted line indicates classic SUV criteria of 2.5 for malignancy diagnosis. $^{***}P < 0.001$.

Performance in Primary Lesions of Lung

As shown in Figure 2A, the ^{18}F-FDG uptake was intense in both NSCLC and TB primary lesions, whereas the ^{68}Ga-Alfatide II uptake in most of the TB lesions was much lower than that in NSCLC lesions.

Quantitative analysis (Fig. 2B) confirmed these results. The ^{18}F-FDG SUV_{max} and SUV_{mean} were not significantly different in NSCLC and TB (SUV_{max}, 10.39 ± 0.88 and 8.40 ± 1.01; SUV_{mean}, 6.49 ± 0.55 and 5.48 ± 0.58, $P = 0.12$ and 0.15, respectively). However, the 2 parameters of ^{68}Ga-Alfatide II were significantly different in NSCLC and TB (SUV_{max}, 3.83 ± 0.22 and 2.29 ± 0.20; SUV_{mean}, 2.90 ± 0.23 and 1.75 ± 0.14, $P = 0.0001$ and 0.0007, respectively). Additionally, all the ^{18}F-FDG SUV_{mean} values of the 34 patients (including all the TB patients) were greater than 2.5.

The ROC curve is shown in Figure 3, and the corresponding statistics are shown in Table 2. The AUC is the highest (0.9011) for ^{68}Ga-Alfatide II SUV_{max} and lowest (0.6502) for ^{18}F-FDG SUV_{mean}. The AUC value of ^{68}Ga-Alfatide II SUV_{max} was significantly higher than that of ^{18}F-FDG SUV_{max} ($Z = 2.068$, $P = 0.038$), and the Youden index was about twice that of ^{18}F-FDG, indicating a higher diagnostic value than ^{18}F-FDG. The cutoff values with a maximum Youden index of the SUV_{max} and SUV_{mean} of ^{68}Ga-Alfatide II and ^{18}F-FDG were 2.75 and 2.15 and 7.30 and 4.75, respectively. When the SUV of the lung lesion shown by either tracer was higher than its cutoff value, we regarded it as NSCLC.

The comprehensive visual analysis showed that the sensitivity, specificity, positive predictive value, and negative predictive value for differentiating NSCLC from TB were 85.71%, 84.62%, 90.00%, and 78.57%, respectively, with ^{68}Ga-Alfatide II and 90.48%, 53.85%, 76.00%, and 77.78%, respectively, with ^{18}F-FDG. The specificity of ^{68}Ga-Alfatide II was 1.57-fold (84.62% vs. 53.85%) that of ^{18}F-FDG, whereas their sensitivities were similar (85.71% vs. 90.48%).

Performance in LNs

In the NSCLC group, 17 of the 21 NSCLC patients who received a resection operation gained a pathologic evidence of LN staging. Eight patients were diagnosed as having LN metastasis.

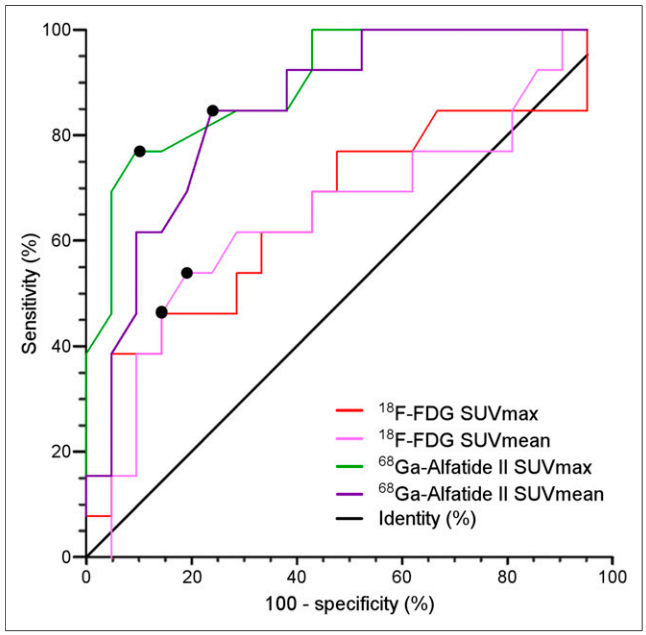

FIGURE 3. ROCs representing discriminatory capability of SUV of ^{18}F-FDG and ^{68}Ga-Alfatide II to differentiate NSCLC from TB lung lesions. Black dots on curves indicate cutoff values for each parameter.

TABLE 2
Performance of ^{68}Ga-Alfatide II for Diagnosis of NSCLC from TB

Analysis	Cutoff value	AUC	Sensitivity (%)	Specificity (%)	Youden index (%)	PPV (%)	NPV (%)
ROC quantitative							
^{68}Ga-Alfatide II	$SUV_{max} < 2.75$	0.9011	76.92	90.48	67.40		
	$SUV_{mean} < 2.15$	0.8535	84.62	76.19	60.81		
^{18}F-FDG	$SUV_{max} < 7.30$	0.6612	46.15	85.71	31.86		
	$SUV_{mean} < 4.75$	0.6502	53.85	80.95	34.80		
Visual analysis							
^{68}Ga-Alfatide II			85.71	84.62		90.00	78.57
^{18}F-FDG			90.48	53.85		76.00	77.78

PPV = positive predictive value; NPV = negative predictive value.

^{68}Ga-Alfatide II PET/CT scanning detected 23 visually positive LNs from 6 patients. These 6 patients were all true-positives. However, ^{68}Ga-Alfatide II failed to identify 2 N stage–positive patients. ^{18}F-FDG detected 34 LNs from 10 patients. Seven of them were true-positives, and 3 were false-positive. Only 1 N stage–positive patient was missed. One of the 3 patients with false-positive ^{18}F-FDG LN staging is shown in Figure 4A.

Statistically, in NSCLC patients, ^{68}Ga-Alfatide II reversed 40% (4/10) of the ^{18}F-FDG–positive LN staging and corrected all the 3 false-positive LN stagings of ^{18}F-FDG but produced 1 false-negative error. ^{68}Ga-Alfatide II was superior to ^{18}F-FDG (100% vs. 66.7%) in specificity, whereas ^{18}F-FDG had a slight advantage in sensitivity (87.5% vs. 75%).

In the TB group, ^{68}Ga-Alfatide II detected 3 false-positive LNs from 2 patients, and ^{18}F-FDG detected as many as 34 false-positive LNs from 6 patients. One typical patient is shown in Figure 4B. The number of false-positive LNs detected by ^{68}Ga-Alfatide II was about one tenth (3/34) of that of ^{18}F-FDG. The LN false-positive rate of ^{68}Ga-Alfatide II was one third (15.4%/46.2%) of that of ^{18}F-FDG.

Performance in Distant Metastasis

In the NSCLC group, 4 patients were clinically diagnosed as having distant metastases. Among them, 2 patients had brain metastasis only, 1 patient had liver + bone metastasis, and 1 patient had brain + liver + bone metastasis (total, 7 brain lesions, 8 liver lesions, and 4 bone lesions). ^{68}Ga-Alfatide II detected 5 additional brain metastases in 2 patients compared with ^{18}F-FDG and changed the metastasis staging in 1 patient. Taking the contralateral normal brain region as a reference, the target-to-non-target SUV_{max} ratio of brain metastasis lesions was 14.3-fold higher (2.06 ± 0.68, $n = 2$ vs. 29.44 ± 4.83, $n = 7$; $P = 0.02$) in ^{68}Ga-Alfatide II images than in ^{18}F-FDG images (Supplemental Fig. 3).

However, ^{68}Ga-Alfatide II failed to detect 3 bone metastases in 2 patients and 7 liver metastases in 1 patient as compared with ^{18}F-FDG and thus mistakenly underestimated the metastasis staging of 1 patient with severe metastasis in the liver and the bone (Supplemental Fig. 4A).

Immunohistochemistry

Immunohistochemistry qualitatively indicated the expression of $\alpha_v\beta_3$ to be predominant in the tumor cells and the vasculature epithelium of the NSCLC samples (Supplemental Figs. 5A and 5B). The TB lesions demonstrate the classic histologic pattern of a tuberculosis granuloma, which is a caseous necrosis in the core, a lymphocyte loop, and a fibrous capsule in the edge (Supplemental Fig. 5C). Both TB granuloma and the surrounding vasculature epithelium showed baseline $\alpha_v\beta_3$ expression (Supplemental Figs. 5C and 5D).

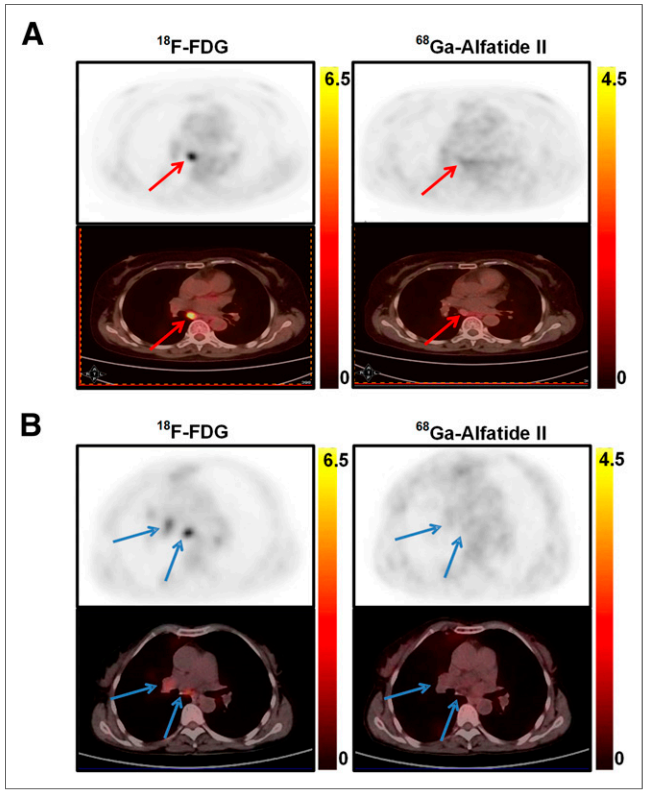

FIGURE 4. (A) Representative transaxial ^{18}F-FDG and ^{68}Ga-Alfatide II PET and PET/CT images of adenocarcinoma patient. Suggestive LNs are indicated by red arrows. ^{18}F-FDG represented positive uptake, whereas ^{68}Ga-Alfatide II represented negative uptake. Postoperative pathology of this LN is benign, and final clinical staging of this patient was T2aN0M0. (B) Representative images of TB patient. Benign reactive LNs are indicated by blue arrows.

DISCUSSION

RGD-based tracers have been clinically explored for oncologic nuclear imaging since 2005 (*15*). Labeled by ^{18}F, ^{68}Ga, or ^{99m}Tc, several RGD-based PET or SPECT tracers have been investigated in a series of landmark clinical trials (*15,22,24–29*). Recently, ^{18}F-NOTA-PRGD2 (denoted as alfatide) has shown to be promising in imaging properties and pharmacokinetics in preclinical or clinical studies (*17–19*). Further research in ^{18}F-Alfatide II (an upgraded version of alfatide) demonstrates great potential of this new tracer in detecting malignant bone and brain metastases (*30,31*). In general, the high detection rate of these RGD-based tracers for detecting primary cancer lesions has been well described by the above clinical studies, but the relatively low sensitivity of this type of tracers for detecting LNs and metastases has also been documented (*32–34*).

In this study, the diagnostic potential of ^{68}Ga-Alfatide II in NSCLC patients was analyzed, and the differential diagnostic value of this new tracer for NSCLC and TB was compared with ^{18}F-FDG. We arrived at the following 3 major conclusions. First, ^{68}Ga-Alfatide II is a qualified molecular imaging tracer for the detection of NSCLC primary lesions and is comparable to ^{18}F-FDG. Second, the differential diagnostic capacity of ^{68}Ga-Alfatide II for NSCLC and TB is superior to that of ^{18}F-FDG both in primary lesions and in suggestive LNs. The optimal criteria of ^{68}Ga-Alfatide II for differentiating NSCLC from TB is an SUV_{max} of 2.75 or greater and an SUV_{mean} of 2.15 or greater. The classic criteria of an ^{18}F-FDG SUV of 2.5 or more for differentiating malignant from benign lesions is of limited applicability for NSCLC and TB. Third, the 2 tracers have their distinct advantages in the detection of distant metastatic lesions. ^{68}Ga-Alfatide II is more likely to be capable of detecting brain metastasis, and ^{18}F-FDG is more likely to be capable of detecting liver and bone metastases.

According to the latest World Health Organization global TB report (http://www.who.int/tb/publications/global_report/en/), developing countries are the main epidemic region of TB in which more than 95% of newly diagnosed cases and death cases are concentrated. Facing the challenge of population migration, HIV infection, multidrug-resistant TB, and environment pollution, TB will remain a severe global health problem in the future (*35*). Our results imply that besides detecting NSCLC lesions, Alfatide II is of additional potential for differentiating NSCLC from TB in TB-epidemic regions. For the patients with suggestive pulmonary lesions, if the personal and epidemic history, clinical manifestations, and laboratory test results indicate a possibility of TB, ^{68}Ga-Alfatide II can be considered for qualitative diagnosis rather than ^{18}F-FDG. Because the inferior sensitivity of ^{68}Ga-Alfatide II for detecting LNs and the metastases on the bone and liver, ^{18}F-FDG is more suitable for the staging and therapeutic monitoring of the diagnosed NSCLC patients.

^{68}Ga-Alfatide II may be better for brain metastasis because of its incapability in passing through the blood–brain barrier, which results in a clear background of normal brain tissue. Our result corroborates the recent research data on ^{18}F-Alfatide II that confirms its capability to detect brain metastasis (*30*).

In bone metastases, it has been noted that ^{68}Ga-Alfatide II seems comparable to ^{18}F-FDG in obvious metastatic lesions (Supplemental Fig. 4B) but is inferior in detecting small early-stage metastases with no obvious abnormal soft tissues (Supplemental Fig. 4A). We suggest the following fact may be the reason for the distinct performance of ^{68}Ga-Alfatide II in different stages of bone metastases. It is the abnormal activation of osteoclasts (which are glucose-avid), the main early-stage pathologic event of bone metastasis (*36*). Then, the process of cancer tissue growth and angiogenesis follows, and the biomarker for RGD targeting starts to be overexpressed.

Some limitations exist in this study. First, because the amount of metastatic NSCLC patients was quite limited, there may be some bias in the result referring the detection of metastatic lesions. Second, immunohistochemistry analysis toward LNs and metastasis is lacking. Third, there are also some other false-positive causes of ^{18}F-FDG, which are not mentioned in this study, such as sarcoidosis, aspergillosis, histoplasmosis, and abscess (*5*). Further investigations are required.

CONCLUSION

^{68}Ga-Alfatide II is qualified for detecting NSCLC primary lesions and is superior to ^{18}F-FDG in distinguishing NSCLC from TB in primary lesions and suggestive LNs. ^{68}Ga-Alfatide II is more likely to be capable of detecting brain metastasis, and ^{18}F-FDG is more likely to be capable of detecting liver and early-stage bone metastases.

DISCLOSURE

The costs of publication of this article were defrayed in part by the payment of page charges. Therefore, and solely to indicate this fact, this article is hereby marked "advertisement" in accordance with 18 USC section 1734. This work was supported by the National Natural Science Foundation of China (grant nos. 81230033, 81401442, 81227901, 81371594, and 81572252) and the Key Science and Technology Program of Shaanxi Province (grant no. 2013K12-03-05). No other potential conflict of interest relevant to this article was reported.

ACKNOWLEDGMENTS

We thank Prof. Xiaoyuan Chen and Prof. Wei Zhang for their generous support and Wansheng Liang, Daliang Liu, Xiaowei Ma, Zhiyong Quan, Guiyu Li, Jin Zeng, Zhiping Yang, Xiaohu Zhao, and Mei Yang for their technical assistance.

REFERENCES

1. Torre LA, Bray F, Siegel RL, Ferlay J, Lortet-Tieulent J, Jemal A. Global cancer statistics, 2012. *CA Cancer J Clin.* 2015;65:87–108.
2. Ettinger DS, Wood DE, Akerley W, et al. Non-small cell lung cancer, version 6.2015. *J Natl Compr Canc Netw.* 2015;13:515–524.
3. Lowe VJ, Fletcher JW, Gobar L, et al. Prospective investigation of positron emission tomography in lung nodules. *J Clin Oncol.* 1998;16:1075–1084.
4. Hashimoto Y, Tsujikawa T, Kondo C, et al. Accuracy of PET for diagnosis of solid pulmonary lesions with ^{18}F-FDG uptake below the standardized uptake value of 2.5. *J Nucl Med.* 2006;47:426–431.
5. Shetty N, Noronha V, Joshi A, et al. Diagnostic and treatment dilemma of dual pathology of lung cancer and disseminated tuberculosis. *J Clin Oncol.* 2014;32:e7–e9.
6. D'souza MM, Mondal A, Sharma R, Jaimini A, Khanna U. Tuberculosis the great mimicker: ^{18}F-fludeoxyglucose positron emission tomography/computed tomography in a case of atypical spinal tuberculosis. *Indian J Nucl Med.* 2014;29:99–101.
7. Prapruttam D, Hedgire SS, Mani SE, Chandramohan A, Shyamkumar NK, Harisinghani M. Tuberculosis: the great mimicker. *Semin Ultrasound CT MR.* 2014;35:195–214.

8. Li Y, Su M, Li F, Kuang A, Tian R. The value of ^{18}F-FDG-PET/CT in the differential diagnosis of solitary pulmonary nodules in areas with a high incidence of tuberculosis. *Ann Nucl Med.* 2011;25:804–811.
9. Sathekge MM, Maes A, Pottel H, Stoltz A, van de Wiele C. Dual time-point FDG PET-CT for differentiating benign from malignant solitary pulmonary nodules in a TB endemic area. *S Afr Med J.* 2010;100:598–601.
10. Chen CJ, Lee BF, Yao WJ, et al. Dual-phase ^{18}F-FDG PET in the diagnosis of pulmonary nodules with an initial standard uptake value less than 2.5. *AJR.* 2008;191:475–479.
11. Shim SS, Lee KS, Kim BT, et al. Non-small cell lung cancer: prospective comparison of integrated FDG PET/CT and CT alone for preoperative staging. *Radiology.* 2005;236:1011–1019.
12. Haroon A, Zumla A, Bomanji J. Role of fluorine 18 fluorodeoxyglucose positron emission tomography-computed tomography in focal and generalized infectious and inflammatory disorders. *Clin Infect Dis.* 2012;54:1333–1341.
13. Kim IJ, Lee JS, Kim SJ, et al. Double-phase ^{18}F-FDG PET-CT for determination of pulmonary tuberculoma activity. *Eur J Nucl Med Mol Imaging.* 2008;35:808–814.
14. Carmeliet P, Jain RK. Angiogenesis in cancer and other diseases. *Nature.* 2000;407: 249–257.
15. Haubner R, Weber WA, Beer AJ, et al. Noninvasive visualization of the activated $\alpha_v\beta_3$ integrin in cancer patients by positron emission tomography and [^{18}F] galacto-RGD. *PLoS Med.* 2005;2:e70.
16. Datta M, Via LE, Kamoun WS, et al. Anti-vascular endothelial growth factor treatment normalizes tuberculosis granuloma vasculature and improves small molecule delivery. *Proc Natl Acad Sci USA.* 2015;112:1827–1832.
17. Guo J, Lang L, Hu S, et al. Comparison of three dimeric ^{18}F-AlF-NOTA-RGD tracers. *Mol Imaging Biol.* 2014;16:274–283.
18. Guo J, Guo N, Lang L, et al. ^{18}F-alfatide II and ^{18}F-FDG dual-tracer dynamic PET for parametric, early prediction of tumor response to therapy. *J Nucl Med.* 2014;55:154–160.
19. Zhu Z, Yin Y, Zheng K, et al. Evaluation of synovial angiogenesis in patients with rheumatoid arthritis using ^{68}Ga-PRGD2 PET/CT: a prospective proof-of-concept cohort study. *Ann Rheum Dis.* 2014;73:1269–1272.
20. Sun Y, Zeng Y, Zhu Y, et al. Application of ^{68}Ga-PRGD2 PET/CT for $\alpha_v\beta_3$-integrin imaging of myocardial infarction and stroke. *Theranostics.* 2014;4:778–786.
21. Peng J, Ouyang Y, Fang WD, et al. Differentiation of intracranial tuberculomas and high grade gliomas using proton MR spectroscopy and diffusion MR imaging. *Eur J Radiol.* 2012;81:4057–4063.
22. Zhu Z, Miao W, Li Q, et al. ^{99m}Tc-3PRGD2 for integrin receptor imaging of lung cancer: a multicenter study. *J Nucl Med.* 2012;53:716–722.
23. Hanley JA, McNeil BJ. A method of comparing the areas under receiver operating characteristic curves derived from the same cases. *Radiology.* 1983;148:839–843.
24. Kenny LM, Coombes RC, Oulie I, et al. Phase I trial of the positron-emitting Arg-Gly-Asp (RGD) peptide radioligand ^{18}F-AH111585 in breast cancer patients. *J Nucl Med.* 2008;49:879–886.
25. Bach-Gansmo T, Danielsson R, Saracco A, et al. Integrin receptor imaging of breast cancer: a proof-of-concept study to evaluate ^{99m}Tc-NC100692. *J Nucl Med.* 2006;47:1434–1439.
26. Kim JH, Lee JS, Kang KW, et al. Whole-body distribution and radiation dosimetry of ^{68}Ga-NOTA-RGD, a positron emission tomography agent for angiogenesis imaging. *Cancer Biother Radiopharm.* 2012;27:65–71.
27. Zheng K, Liang N, Zhang J, et al. ^{68}Ga-NOTA-PRGD2 PET/CT for integrin imaging in patients with lung cancer. *J Nucl Med.* 2015;12:1823–1827.
28. Mittra ES, Goris ML, Iagaru AH, et al. Pilot pharmacokinetic and dosimetric studies of ^{18}F-FPPRGD2: a PET radiopharmaceutical agent for imaging $\alpha v\beta 3$ integrin levels. *Radiology.* 2011;260:182–191.
29. Gao S, Wu H, Li W, et al. A pilot study imaging integrin $\alpha_v\beta_3$ with RGD PET/CT in suspected lung cancer patients. *Eur J Nucl Med Mol Imaging.* 2015; 42:2029–2037.
30. Yu C, Pan D, Mi B, et al. F-Alfatide II PET/CT in healthy human volunteers and patients with brain metastases. *Eur J Nucl Med Mol Imaging.* 2015;13:2021–2028.
31. Mi B, Yu C, Pan D, et al. Pilot Prospective evaluation of ^{18}F-alfatide II for detection of skeletal metastases. *Theranostics.* 2015;5:1115–1121.
32. Beer AJ, Grosu AL, Carlsen J, et al. [^{18}F]galacto-RGD positron emission tomography for imaging of $\alpha_v\beta_3$ expression on the neovasculature in patients with squamous cell carcinoma of the head and neck. *Clin Cancer Res.* 2007;13: 6610–6616.
33. Beer AJ, Niemeyer M, Carlsen J, et al. Patterns of $\alpha_v\beta_3$ expression in primary and metastatic human breast cancer as shown by ^{18}F-galacto-RGD PET. *J Nucl Med.* 2008;49:255–259.
34. Axelsson R, Bach-Gansmo T, Castell-Conesa J, McParland BJ, Study G. An open-label, multicenter, phase 2a study to assess the feasibility of imaging metastases in late-stage cancer patients with the alpha v beta 3-selective angiogenesis imaging agent ^{99m}Tc-NC100692. *Acta Radiol.* 2010;51:40–46.
35. Cobelens F, van Kampen S, Ochodo E, Atun R, Lienhardt C. Research on implementation of interventions in tuberculosis control in low- and middle-income countries: a systematic review. *PLoS Med.* 2012;9:e1001358.
36. Coleman RE. Metastatic bone disease: clinical features, pathophysiology and treatment strategies. *Cancer Treat Rev.* 2001;27:165–176.